RC24405 (W0711-040) November 7, 2007
Materials Science

IBM Research Report

Ultralow Dielectric Constant pSiCOH Films Prepared with Tetramethylcyclotetrasiloxane as Skeleton Precursor

A. Grill, V. Patel
IBM Research Division
Thomas J. Watson Research Center
P.O. Box 218
Yorktown Heights, NY 10598

Research Division
Almaden - Austin - Beijing - Cambridge - Haifa - India - T. J. Watson - Tokyo - Zurich

Ultralow dielectric constant pSiCOH films prepared with tetramethylcyclotetrasiloxane as skeleton precursor.

A. Grill and V.Patel

IBM – T. J. Watson Research Center, Yorktown Heights, NY 10598

ABSTRACT

Ultralow dielectric constant pSiCOH films have been prepared using tetramethylcyclotetrasiloxane (TMCTS) as the skeleton precursor and two different porogen precursors. The porogen has been removed from the deposited films by thermal anneals at 400 ^{o}C, obtaining films with dielectric constants down to 1.95. The films have been investigated by Fourier transform infrared spectroscopy (FTIR) and n&k optical measurements of the refractive index (n) and the electrical characteristic have been measured on metal-insulator-semiconductor (MIS) structures. It was found that the properties of the annealed films depend on the deposition temperature and on the used porogen, different concentrations of porogens in the plasma feed being required to obtain the same final dielectric constant. The efficiency of porogen incorporation in the films prepared from TMCTS was very low and was dependent on the selected porogen precursor.

I. INTRODUCTION

The shrinkage of VLSI devises has lead to the need to replace the silicon dioxide interconnect dielectric with materials of lower dielectric constants. After many efforts, the organosilicate glass SiCOH dielectric prepared by plasma enhanced chemical vapor deposition (PECVD) and having a dielectric constant, k ~3.0 [1] has been demonstrated already in 1999 and has finally been introduced at the 90 nm node and adopted generally by the industry by 2004 (see a review in [2]). The semiconductor industry expected a further decrease of the dielectric constant with each new generation node. The reduction of k of SiCOH can be achieved by introducing porosity in the films and this can be done either by adjusting the parameters of the PECVD process, or by a subtractive process whereby a labile fraction of the deposited film is removed after its deposition. While the dielectric constant of SiCOH has been lowered to k=2.75 by the first approach [3] that produced an integratable film [4], the second approach is much more flexible. As already described in 2000 [5, 6], porous pSiCOH films can be prepared by adding a porogen precursor to the SiCOH precursor in the plasma feed, depositing a dual phase film SiCOH-CH and removing the less stable CH fraction by curing the film. Using a thermal cure, pSiCOH films with k=1.95 have been demonstrated in the lab [7] and an advanced film ready for integration at 45 nm has been reported in 2006 [8, 9].

A variety of cyclic or linear molecules can be used as SiCOH precursors [10, 11], such as tetramethylcyclotetrasiloxane (TMCTS) [12], octamethylcyclotetrasiloxane (OMCTS) [13], decamethylcyclopentasiloxane (DMCPS) [14, 15], or diethoxymethylsilane (DEMS) [16]. Any hydrocarbon with sufficient volatility to enable delivery as a gas to the PECVD reactor could in principle be used as a porogen. However the requirement [7], that the rf power has to be kept at a sufficiently low level to prevent

excessive dissociation of the skeleton precursor and produce a pure SiCOH film with k≤3.0 and yet be sufficiently high to dissociate the porogen precursor, limits the choices of skeleton-porogens combinations. The hydrocarbons that could be used as porogen need to have some weak bonds that are easily dissociated in the low power plasma and these comprise cyclic unsaturated hydrocarbons, e.g. terpinenes or norborenes, linear alkenes, or molecules with strained rings, e.g. cycloalkene oxides [11, 14, 17].

Taking into account the multiplicity of precursor choices and the complexity of the deposition of pSiCOH films, the purpose of this study was to investigate the effect of some plasma parameters and the choice of porogen on the deposition and properties of pSiCOH. We chose TMCTS as the skeleton precursor because it was found previously that cyclic precursors produce non porous SiCOH films with superior mechanical properties [18] and, among the cyclic precursors, TMCTS has sufficient volatility to be delivered as a gas to our custom built reactor. Two porogen have been chosen for this study, namely cyclopentene oxide (CPO) and butadiene monoxide (BMO).

II. EXPERIMENTAL

The pSiCOH films investigated in this study have been prepared as described previously [5] in an 8" parallel plate, RF powered, PECVD reactor. The deposition was performed on Si(100) wafers placed on a electrode that could be heated up to 180 ^{o}C. Most of the films were deposited at a RF power of 15 W and a pressure of 500 mtorr. Some films were deposited at different powers when so specified.

TMCTS ($T_{boiling}$ = 135 ^{o}C) was used as the SiCOH skeleton precursor and was delivered to the reactor flowing He through a bubbler containing the liquid at room

temperature. The total flow rate was controlled by a mass flow controller (MFC) and the flow rate of TMCTS was calculated using the equation

$$Q_{TMCTS} = P_{TMCTS}/P_{total}*Q_{total}$$

where Q = flow rate and P = pressure. The vapor pressure of TMCTS (P_{TMCTS}) at 25 ^{o}C is 9 torr [19] and the total pressure in the bubbler was 1000 torr.

The porogen precursors, cyclopentene oxide (CPO) with $T_{boiling}$ = 102 ^{o}C and butadiene monoxide (BMO) with $T_{boiling}$ = 65 ^{o}C have sufficient vapor pressure at room temperature to be delivered directly to the reactor though the corresponding MFCs. Both porogens have been selected because they contain a strained C-C-O ring in their molecules and it was expected that the bonds of this ring will dissociate easy in the plasma creating radicals that could be incorporated as the CH phase in the SiCOH skeleton. The BMO molecule contains in addition an unsaturated C=C bond which could dissociate relatively easy in the plasma. The porogen precursors were delivered to the reactor at different flow rates defined as

R = (porogen flow rate) / (TMCTS flow rate)

and the results will be discussed in terms of R values. The structures of the used precursors are illustrated in Figure 1.

After deposition, the porogen was removed from the films by annealing them in He at 400 ^{o}C for 4 hours. Some films were annealed at 430 ^{o}C. Unless otherwise specified, the anneals in the discussion of the results will refer to the 400 ^{o}C anneal.

The structure of the films was characterized by Fourier transform infrared spectroscopy (FTIR) and the refractive index (n) and optical gap (E_{opt}) were determined by n&k measurements [20]. Film thickness was measured with a profilometer in steps

created in the film and the she shrinkage of the films during annealing was determined by measuring the thickness of the as-deposited and annealed films. The error in the shrinkage values is +/- 1.5%. The dielectric constant was measured on metal-insulator-semiconductor (MIS) structures using Al dots evaporated on the film and Al metallization of the back of the Si wafers. The electrical measurements were performed at 150 ^{o}C to remove any humidity physisorbed in the porous films. The error in the values of the dielectric constant is +/- 0.05.

III. RESULTS and DISCUSSION

III.A. pSiCOH deposited from TMCTS + CPO

III.a.1. Effect of deposition temperature

The deposition of films by the PECVD technique is controlled mostly by the energy of the electrons in the plasma [21]. Collisions of the electrons with the precursor molecules in the gas (plasma) phase cause the dissociation and ionization of these molecules creating active species (ions and radicals) which diffuse to the substrate where they react and form a film. Contrary to the CVD method, in PECVD the substrate does not have to be heated to a high temperature which is sufficient to react the precursor molecules and form a solid film. Nevertheless, the substrate temperature in PECVD can affect the concentration of the reactive species on the substrate and their kinetics, thereby affecting the properties of the deposited film and its behavior when exposed afterward to higher temperatures. For the preparation of porous films, where the porogen is removed by annealing at temperatures of 400 ^{o}C or more, the substrate temperature has to be

significantly lower to incorporate sufficient porogen species. In the PECVD reactor used for the present study the highest substrate temperature was 180 ^{o}C and we compared initially films deposited at 100 ^{o}C, 140 ^{o}C and 180 ^{o}C.

III.A.1.1. FTIR analysis

We used FTIR spectroscopy to study structural differences between films deposited under different conditions. For a given chemistry, the CH_i absorption band centered at about 2950 cm^{-1} [12] scales with the amount of organic porogen incorporated in the film and can thus be used to compare porogen incorporations in different films. Figure 2 compares the FTIR spectra of films deposited from TMCTS + CPO at the three temperatures mentioned above and at a porogen to precursor flow ratio R(CPO) = 55.6. Figure 3 compares the spectra of the same films after annealing them at 400 ^{o}C for 4 hours. Figures 2.a and 3.a show the full spectra normalized to same SiO peak (~1050 cm^{-1}) intensity. Figures 2.b and 2.c show expanded wavenumber sections of Figure 2.a at same relative intensities. The CH_i absorption band in Figure 2.b (see [12] for identification of the different absorption peaks) indicates that the amounts of organic porogen incorporated in the films decrease with increasing deposition temperature. As we will show later, the amounts of incorporated porogen will affect the shrinkage of the films and their dielectric constant (k) values after annealing. Figure 2.c shows that the deposition temperature also affects the structure of the SiO band (1048-1136 cm^{-1}), whose width is related to the relative amounts of cage type and network type oxide bonds. The deconvolution of the SiO absorption bands into different type of oxide components

can be found elsewhere [12]. The absorption peak at 905 cm^{-1} indicates that more hydrogen is incorporated in the films as H-SiO_3 with decreasing deposition temperature.

A strong decrease in the intensity of the CH_i band after annealing is observed for all the films in Figure 3, indicating the removal of the organic porogen during annealing. The intensity of the CH_i band in the annealed film is only slightly dependent on the deposition temperature indicating that all films contain about same amount of residual organic fraction. The expanded spectra in Figure 3.c show some differences in the oxide band whose peak is shifting to higher wavenumbers with increasing deposition temperature and shows a slightly lower concentration of Si-CH_3 (SiMe) bonds (peak at 1271 cm^{-1}) in the film deposited at the highest temperature.

III.A.1.2. Shrinkage and Dielectric constant

Removal of porogen during annealing causes the formation of porosity in the films but also results in film shrinkage. The degree of porosity in the annealed film, which depends on the amount of shrinkage, it will decrease, and the dielectric constant will increase if the shrinkage is too large [22]. The differences in porogen incorporation in the films deposited at different temperatures affect the shrinkage of the films during annealing and their final dielectric constants. Figure 4 presents the shrinkage of the films after annealing at 400 ^oC vs. the deposition temperature for films deposited from TMCTS+CPO at two R values. The shrinkage decreases with increasing deposition temperature for both R values, or, referring the previous FTIR discussion, the shrinkage decrease with decreasing porogen incorporation in the as-deposited film.

The different slopes of shrinkage vs T for the two different R values are most probably caused by the interaction of the plasma parameters which could be affected by different total flows.

The dielectric constant of the annealed films follows the same trend as the shrinkage, as shown in Figure 5. The trend lines for the two different R values seem to cross-over, however the plot of all dielectric constants vs. shrinkage in Figure 6 shows a direct correlation between shrinkage and dielectric constant, k increasing with increasing shrinkage. The deviations of the symbols from the trend line in this plot are due to experimental errors in k and shrinkage measurements,. Thus, while deposition from the same plasma chemistry at a lower substrate temperature results in a larger amount of incorporated porogen, removal of the larger amount of porogen causes a larger shrinkage of the film. A similar behavior was observed for films deposited from octamethylcyclotetrasiloxane (OMCTS) and CPO [13]. The results show that there is a competition between the formation of porosity by removal of porogen and the densification of the film by its shrinkage. The films deposited at lower temperature have lower degree of porosity after annealing than the films deposited at higher temperature as reflected by the higher k values after annealing.

The results discussed above show that deposition at higher substrate temperature is preferable for obtaining a lower k value and lower shrinkage, the latter meaning higher throughput in manufacturing. The rest of the study was performed on films deposited on substrates at 180 ^{o}C and the data discussed next was obtained for such films.

III.A.2. Effect of CPO concentration (R)

III.a.2.1. FTIR analysis

The effect of the amount of the CPO porogen precursor in the plasma feed is illustrated in Figures 7 and 8 which present FTIR spectra of films deposited from mixtures with different R(CPO) values. The two figures include the spectra of films deposited from TMCTS only, without any porogen. It can be seen that the spectrum of the film deposited at R=0 has a very low CH_i absorption band and has also a SiH_i absorption band at about 2200 cm^{-1} [12]. The addition of CPO to the plasma feed eliminates almost completely the SiH_i band, increases strongly the CH_i band and, for the higher R=33.3, it increases the SiMe (Me = CH_3) peak at 1271 cm^{-1}. In the same time, the width of the SiO absorption band increases with increasing R, indicating an increase in the cage SiO fraction, and shifts towards higher wavenumbers (Figure 7.b). A splitting of the SiO peak is observed for R=33.3 indicating a large fraction of the cage type oxide.

The effect of R on the structure of the annealed films is shown in Figure 8. The relative intensity of the CH_i band of all TMCTS+CPO based films is strongly reduced as compared to the as-deposited films, its intensity is almost independent on the R value, but it is still higher than the intensity of the peak of the film deposited without porogen (R=0). Only the film deposited with the largest R=55.5 has a slightly higher CH_i peak in the annealed film (See Figure 8.b). The effect of the CPO fraction in the plasma feed on the SiO band of the annealed films can be seen in the enlarged section of the spectra in Figure 7.c. In addition to the broadening of the peak and it shift to higher wavenumbers with increasing R, as observed in the as-deposited film, the SiMe peak at 1271 cm^{-1} of the annealed film increases continuously with increasing R. Since the SiMe groups are

terminal groups, creating porosity around them, the above observation indicates that the degree of porosity in the annealed films increases with increasing R values.

III.A.2.2. Refractive index and Optical gap.

The refractive index (n) and optical gap (E_{opt}) are summarized in Table I as a function of R(CPO). The optical gap of the as-deposited films (E_{opt}-d) is essentially constant at about 4 eV, but increases for the annealed films (E_{opt}-A) from 3.16 eV to 3.6 eV with increasing fractions of porogen (R) in the plasma feed. The differences in values of E_{opt}-d are most probably due to experimental errors.

The refractive index displays a similar behavior to the optical gap. It is essentially constant at ~1.50 for the as-deposited films (n-dep), independent on R, and the differences in the values of n are most probably a result of experimental errors. Contrary to that, the refractive index of the annealed films (n-A) decreases continuously from 1.49 to 1.34 with increasing R. The decrease in n reflects the reduction of film density (increase in porosity) and indicates a reduction in dielectric constant of the annealed films prepared with increasing fractions of porogen (R) in the plasma feed.

III.A.2.3. Dielectric constant and leakage current

Based on the above discussion it is expected that the dielectric constant of the films deposited from TMCTS+CPO and annealed at 400 ^{o}C will decrease with increasing fraction of porogen in the plasma feed (R). The expected behavior is indeed shown in Table II which presents k of the pSiCOH films deposited with different R values after annealing at 400 ^{o}C for 4 hours (k(A)). The amount of porogen incorporated in the films

increases with increasing R, as discussed above in section III.A.2.1, and the shrinkage of the films during annealing is sufficiently limited to result in increasing porosity with increasing R for the conditions investigated in this study. As a result both the dielectric constant k and the refractive index n decrease with increasing R(CPO). As can be seen in Table II, a value as low as k(A)=2.05 was obtained for the films deposited at the highest R=55.6.

A typical plot of leakage current vs. electric field in these pSiCOH films can be found elsewhere [7]. The breakdown field of a film with k=2.45 is 5.5 MV/cm and typically decreases with the decreasing k, but the leakage current at fields below 2 MV/cm is about the same for all investigated films prepared from TMCTS+CPO. The low current leakage of $1E^{-9}$ A/cm^2 at 1 MV/cm would make these films suitable for integration in an interconnect structure.

III.B. pSiCOH deposited from TMCTS+BMO films

III.B.1. FTIR analysis

In order to compare the effect of porogen on the deposition and properties of the ultralow-k (ULK) films we replaced the CPO porogen with BMO. Figures 9 and 10 compare the FTIR spectra of films deposited at two values of R(BMO) with that of a films deposited at R(CPO) = 55.6. The CH_i peak in Figure 9, presenting spectra of as-deposited films, shows that, at same R = 55.6, much less porogen is incorporated in the TMCTS+BMO based film than in TMCTS+CPO based film. R(BMO) has to be increased to 83.3 to obtain about same amount of porogen incorporation as in the film prepared with R(CPO)=55.6. Furthermore, the replacement of CPO with BMO results in

a somewhat narrower SiO absorption band with the peak shifted to lower wavenumbers (Figure 9.c).

The spectra of the annealed films in Figure 10 show small differences in the residual CH_i absorption band, the main differences being a higher sp^3 absorption peak at 2970 cm^{-1} in the film deposited with R(BMO) = 83.3. The differences in the SiO absorption bands of the annealed films in Figure 10.c are the same as discussed above for the as-deposited films, indicating differences in the O-Si-O bonding angles [12] between the films deposited with different porogens: the films deposited with BMO have smaller O-Si-O angles than the films deposited with CPO [12]. Figure 10.c also shows a small shoulder at ~1260 cm^{-1} in the SiMe peak (at ~1272 cm^{-1}) corresponding to $SiMe_2$ absorption, in the spectra of the pSiCOH films deposited with BMO. This indicates that the BMO porogen resulted in the formation of a fraction of $SiMe_2$ bonds in addition to the SiMe bonds. Such $SiMe_2$ absorption has not been observed in the films deposited from TMCTS+CPO.

The results presented above show that, for films prepared from the same skeleton TMCTS precursor, the incorporation efficiency of porogen in the as-deposited film depends on the used porogen and the structure of the annealed porous films can also be affected by the used porogen.

III.B.2. Dielectric constants

The dielectric constants of the annealed TMCTS+BMO films are shown as a function of power and R(BMO) in Figure 11 and compared at the same power with films deposited from TMCTS+CPO in Table III. As shown in Figure 11, the dielectric constant increases with the deposition power for both R(BMO) values and lower k values are

obtained for the larger R, similar to films deposited with CPO. Table III, which presents the k values for all films deposited at a power of 15 W, shows again that R(BMO) values much higher than R(CPO) are required to obtain the same dielectric constant. For example, k=2.35 was obtained with R(CPO) =33.3 but R(BMO)=55.6. Furthermore, while the FTIR spectra in Figure 9 indicated that similar amounts of porogen were incorporated at R(CPO)=55.6 and R(BMO)=83.3, a lower dielectric constant was obtained for the films deposited with CPO (k=2.07) as compared to the films deposited with BMO (k=2.27) at the corresponding R values.

The results presented above show that for the same skeleton precursor (TMCTS in present study) the used porogen can affect: i) the incorporation efficiency of the porogen; ii) the structure of the annealed porous films; iii) the dielectric constant of the annealed pSiCOH. Furthermore, the incorporation of porogens in films deposited with TMCTS as the SiCOH skeleton precursor is very inefficient for both studied CPO and BMO porogens. Very high porogen to skeleton precursor flow ratios are required to obtain ULK films. R(CPO) >33 or R(BMO)>55 are required to obtain pSiCOH with k<2.4 and such R values are too high for manufacturing purposes and a different SiCOH skeleton precursor has to be chosen for practical applications.

III.C. Annealing at 430 ^{o}C

The 4 hour anneal at 400 ^{o}C resulted in the removal of most porogen from the investigated pSiCOH films, however it was found that this anneal is not sufficient to remove all porogen. While ultralow-k values have been obtained for the TMCTS+CPO

film annealed for 4 hr at 400 ^{o}C, the k values of same films could be further lowered by a second identical anneal. This is illustrated in Table II that compares the k(A) values after one anneal with corresponding k(AA) values after a double anneal and a value as low as k(AA)=1.95 was obtained for R(CPO)=55.6. The decrease of k after the second anneal indicates that the second anneal at 400 ^{o}C further increased the porosity in the film by removal of residual porogen.

These results indicated that a higher thermal budget than the 4 hours at 400 ^{o}C is required to completely remove the porogen from the deposited films and an anneal of 4 hours at 430 ^{o}C was later investigated.

The removal of porogen from the TMCTS+CPO based films as a function of time, between 0 and 4 hours, at 430 ^{o}C was studied by comparing the FTIR spectra of the films as shown in Figure 12. The films were deposited from TMCTS+CPO with R(CPO = 55.6. The CH_i absorption band centered at ~ 2950 cm^{-1} and the oxide band at ~1100 cm^{-1} show that most of the porogen is removed from the films and most changes occur in the oxide bonds during the first hour of annealing at 430 ^{o}C. Nevertheless some significant changes are still observed to occur in the CH_i and SiO peaks during the second hour of annealing. Much smaller changes are observed during the third hour and no changes were observed during the fourth hour. The intensity of the SiMe peak at 1270 cm^{-1} decreases slightly after 1st hour of annealing and no detectable change are observed in this peak with longer anneal times (Figure 12.c).

A similar behavior of structural changes with annealing time at 430 ^{o}C was observed for films deposited from TMCTS +BMO. Furthermore, a second anneal for 4 hours at 430 ^{o}C did not produce any detectable changes in the FTIR spectra or in the k values as

compared to the first identical anneal. Based on these results it was concluded that an anneal of 4 hours at 430 ^{o}C should be sufficient to remove all labile porogen from the pSiCOH films and such an anneal was adopted for subsequent studies.

IV. CONCLUSIONS

ULK pSiCOH films have been prepared by thermally annealing films deposited from TMCTS and two different porogen precursors, namely CPO and BMO. The incorporation of porogen in the films and their properties were affected by the deposition temperature and, for films deposited with CPO porogen, lower deposition temperature resulted in larger shrinkage during anneal and larger dielectric constants.

For both porogen precursors the incorporation in the films had low efficiency as very large concentrations R of porogen precursor in the plasma feed was required to obtain ULK films. Much larger R(BMO) than R(CPO) was required to obtain films of similar k values. Dielectric constants down to 1.95 have been obtained at the largest concentration of CPO in the plasma feed.

The anneal of 4 hours at 400 ^{o}C proved to be insufficient for complete removal of the porogen form the films. An anneal of 4 hours at 430 ^{o}C was found to remove completely the porogens and produce stable films.

The high ratio of porogen to SiCOH skeleton precursor required to obtain ULK films based on TMCTS makes this skeleton precursor unattractive for commercial applications. Another skeleton precursor that would require significantly lower porogen precursor is needed for practical fabrication of ULK pSiCOH BEOL dielectrics.

REFERENCES

1. A. Grill, L. Perraud, V. Patel, C. Jahnes, and S. Cohen, Mat.Res.Soc. Symp.Proc., **565** (1999) 107.
2. A. Grill, Ch.1 in "Dielectric Films for Advanced Microelectronics", eds. M. Baklanov, M. Green and K. Maex, John Wiley & Sons, West Sussex, England, 2007.
3. K. Ida, S. Nguyen, S. Lane, N. Klymko, K. Chanda, F. Chen, C. Christiansen, S. Cohen, M. Cullinan, C. Dziobkowski, M. Fukasawa, A. Grill, K. Inoue, K. Kumar, M. Lane, E. Liniger, V. McGahay, K. Malone, M. Minami, D. Restaino, A. Sakamoto, M. Sankar, M. Sherwood, E. Simonyi, Y. Shimooka, J. Widodo, H. WILDMAN, M. Ono, D. McHerron, H. Nye, D. Edelstein, T. Nogami and T. Ivers, Conf. Proc.AMC XXI (2006) 89, Mat.Res.Soc.
4. V. McGahay, G. Bonilla, F. Chen, C. Christiansen, M. Cullinan-Scholl, J. Demarest, D. Dunn, J. Fitzsimmons, J. Gill, S. Grunow, K. Ida1, M. Kiene, C. Labelle, E. Liniger, X.H. Liu, K. Malone, P.V. McLaughlin, M. Minami1, S. Molis, C. Muzzy, S. Nguyen, A. Sakamoto, T.M. Shaw, E. Simonyi, A. Grill, R. Hannon, M. Lane, T. Nogami1, H. Nye, M. Ono, T. Spooner, and T. Ivers, Proceedings of the IEEE 2006 Intern. Interconnect Technol. Conference, IEEE, Piscataway, NJ (IEEE Catalog No. 06TH8862) (2006) p 9.
5. A. Grill and V. Patel, Electrochemical Soc.Proc., **2000-5** (2000) 55.
6. US patent 6,312,793 issued Nov. 6 , 2001.
7. A. Grill and V. Patel, Appl.Phys.Lett., **79**, 803 (2001).

8. S. Gates, A. Grill, C. Dimitrakopoulos, D. Restaino, M. Lane, V. Patel, S. Cohen, E. Simonyi, E. Liniger, Y. Ostrovski, R. Augur, M. Sherwood, N. Klymko, S. Molis, W. Landers, D. Edelstein, S. Sankaran, R. Wisnieff, T. Ivers, K. Yim , S. Ahn, T. Nowak, J. Rocha, K. Chan, S. Yi, N. Rajagopalan, G.Balasubramanian, S. Reiter, A. Demos, AMC 2006, Paper Number VII.3.
9. S. Sankaran, S. Arai, R. Augur, M.Beck, T. Bolom, G. Bonilla, O. Bravo, K. Chanda, L. Clevenger, S.Cohen, P. Davis, C. Dimitrakopoulos, R. Filippi, J. Fitzsimmons, P. Flaitz, S. Greco, S. Grunow, K. Ida, D.Y .Jung, M. Kelling, T. Ko, K. Kumar, C. Labelle, W. Landers, M. Lee, W. Li, X. Liu, W.Lu, N. Lustig, K. Malone, S.Marokkey, P.S. McLaughlin, P.V. McLaughlin, K. Miyata, D. Nguyen, L. Nicholson, D. Nielsen, P. Ong, K. Patel, W.Park, S. Ponoth, K. Petrarca, D. Rath, D. Restaino, S. Rhee, H. Shoba, T. Standaert, C. Tian, H.Wendt, J, Werking, J.Widodo, T. Spooner, A. Grill, A. Cowley, R. Hannon , J. Pellerin, D. Edelstein, G. Biery, T. Ivers , IEDM 2006, paper S13P2.
10. A. Grill, Proc. 23rd VMIC, Sept.26-28, 2006, Freemont, CA, p165.
11. V. Ruessac, L.Favennec, B. Remiat, V. Jousseaume, G. Passemard and J. Durand, Microelectronic Engineering, **82**, 333 (2005).
12. A. Grill and D. Neumayer, J.Appl. Phys., **94**, 6697 (2003).
13. S.M. Gates, D. Neumayer, H.M. Sherwood, A. Grill, X. Wang and M. Sankarapandian, J. Appl.Phys., **101**, 094103 (2007).
14. L.Favennec, V. Jousseaume, V. Ruessac, F. Fusalba, J. Durand, G. and Passemard, Mater. Sci. Semicond. Process. **7**, 277 (2004).

15. J. Yang, S. Lee, H. Park and D. Jung, J.Vac,Sci.technol. H. Chae, **A24**, 165 (2006).
16. R. Vrtis, M. O'Neill, J. Vincent, L. Lukas, B. Peterson, M.Bitner, E. Karwacki, Mat.Res.Soc. Symp.Proc. **766**, 259 (2003).
17. US Patent 6,441,491, issued Aug.27, 2002.
18. A. Grill, D. Edelstein and V. Patel, Conf. Proc. **ULSI XVII** 253 (2002) Mat.Res.Soc.
19. Ultrapur TMCTS, © 2000 ATMI, Inc. 617 River Oaks Parkway, San Jose , CA 95134.
20. n&k Analyzer 1280 from n&k Technology, Inc. 4051 Burton Drive, Santa Clara, California, 95054.
21. A. Grill, Cold Plasma in Materials Fabrication: From Fundamentals to Applications, IEEE Press, New York, 1994: Wiley-IEEE Press, Hoboken, NJ, March 2001.
22. A. Grill, J.Appl.Phys., **93**, 1785 (2003).

Table I: Optical gap and refractive index of films prepared with CPO.

R(CPO)	E_{opt}-d (eV)	E_{opt}-A (ev)	n_{dep}	n_A
18.5	4.00	3.16	1.52	1.49
22.2	4.00	3.14	1.51	1.48
33.3	4.03	3.21	1.50	1.44
38.9	4.09	3.36	1.49	1.41
44.4	4.08	3.46	1.50	1.38
55.6	3.98	3.60	1.50	1.34

Table II: Dielectric constants of films prepared with CPO after first and second anneal at 400 ^{o}C.

R(CPO)	k(A)	k(AA)
22.2	2.45	2.3
33.3	2.35	2.15
44.4	2.21	2.09
38.9	2.24	2.09
55.6	2.07	1.95

Table III: Dielectric constants vs. porogen concentration in plasma feed.

R	11.1	18.5	27.8	11.1	22.2	33.3	44.4	38.9	55.6	83.3
Porogen	**Dielectric constant - k(A)**									
CPO	2.77	2.57	2.44	2.77	2.45	2.35	2.21	2.24	2.07	
BMO									2.36	2.27

Figure Captions

Figure 1: Structures of molecules used in the present study.

Figure 2: FTIR spectra of as-deposited pSiCOH films prepared from TMCTS+CPO at different substrate temperatures, at R(CPO) = 55.6. a) full spectra; b) and c) expanded sections of the spectra.

Figure 3: FTIR spectra of annealed pSiCOH films prepared from TMCTS+CPO at different substrate temperatures, at R(CPO) = 55.6. a) full spectra; b) and c) expanded sections of the spectra.

Figure 4: Shrinkage during anneal of pSiCOH films deposited at two R(CPO) values vs. deposition temperature.

Figure 5: Dielectric constants of annealed pSiCOH films deposited at two R(CPO) values vs. deposition temperature.

Figure 6: Dielectric constants vs. shrinkage of the films from Figures 4 and 5.

Figure 7: FTIR spectra of as-deposited pSiCOH films prepared from TMCTS+CPO at different R values and 180 ^{o}C. a) full spectra; b) and expanded section of the spectra. The film at R=0 was-deposited at 5W, because at higher power TMCTS was dissociated too much and the obtained k value was high.

Figure 8: FTIR spectra of annealed pSiCOH films prepared from TMCTS+CPO at different R values and 180 ^{o}C. a) full spectra; b) and c) expanded sections of the spectra.

Figure 9. FTIR spectra of as-deposited films prepared from TMCTS+CPO and TMCTS+BMO at different R values and 180 ^{o}C. a) full spectra; b) and c) expanded sections.

Figure 10. FTIR spectra of annealed films prepared from TMCTS+CPO and TMCTS+BMO at different R values and 180 ^{o}C. a) full spectra; b) and c) expanded sections.

Figure 11. Dielectric constants of annealed TMCTS+BMO films prepared at two R(BMO) values vs. RF deposition power.

Figure 12. FTIR spectra of films deposited from TMCTS+CPO at R(CPO)= 55.6 and and 180 ^{o}C as a function of annealing time at 430 ^{o}C. a) full spectra; b) and c) expanded sections.

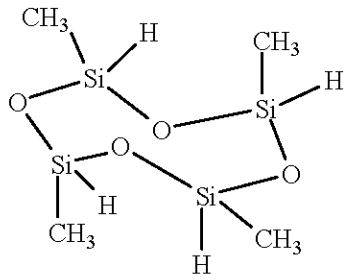

TMCTS

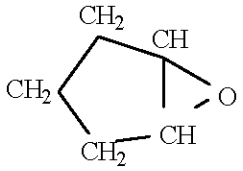

CPO

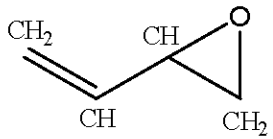

BMO

Figure 1

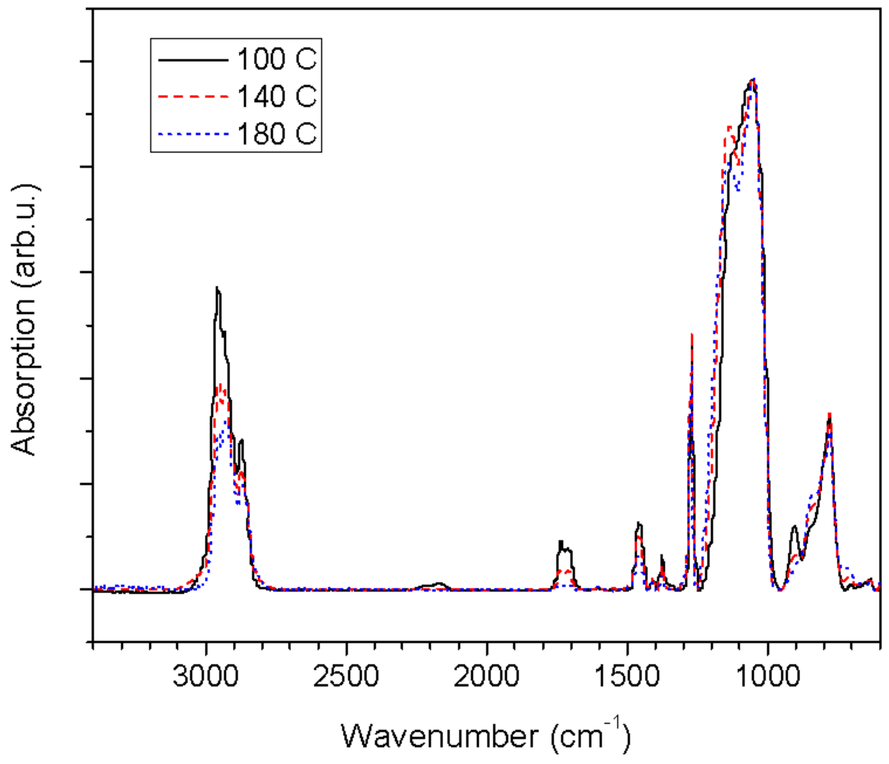
100 C
140 C
180 C
Absorption (arb.u.)
3000
2500
2000
1500
1000
Wavenumber (cm-1)

Figure 2.a

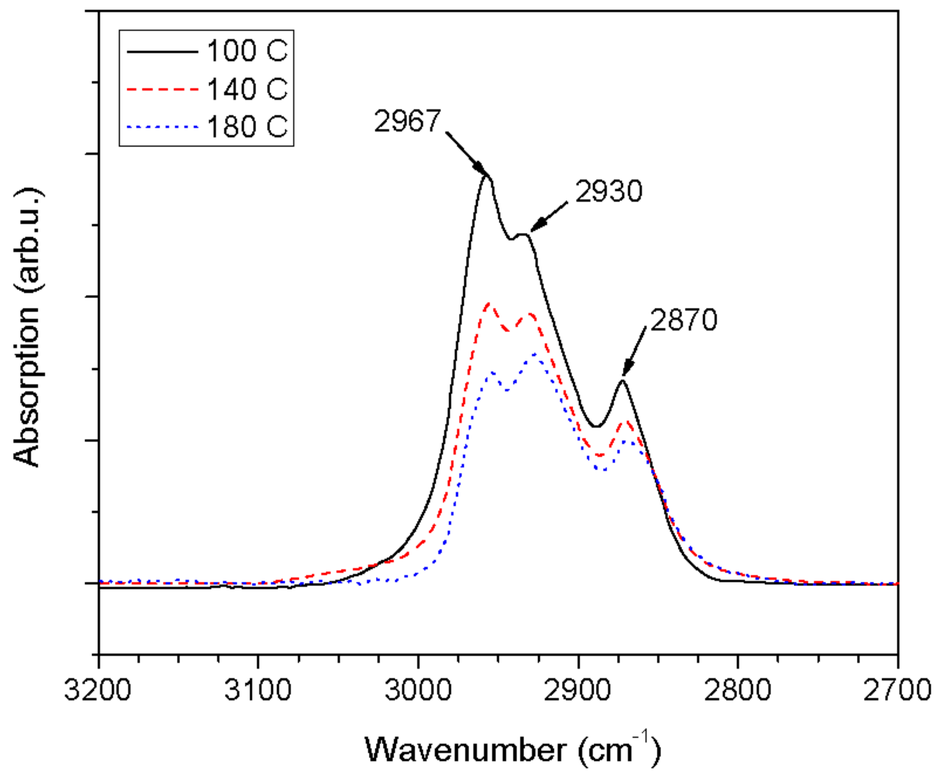
100 C
140 C
180 C
2967
2930
2870
Absorption (arb.u.)
3200
3100
3000
2900
2800
2700
Wavenumber (cm-1)

Figure 2.b

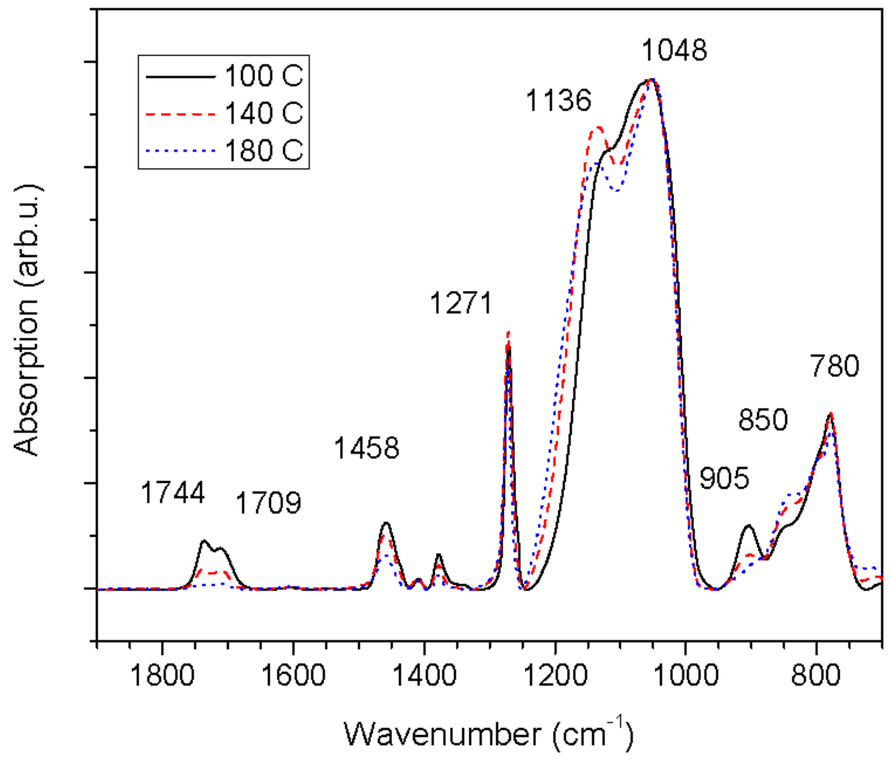
100 C
140 C
180 C
1744
1709
1458
1271
1136
1048
905
850
780
Absorption (arb.u.)
1800
1600
1400
1200
1000
800
Wavenumber (cm-1)

Figure 2.c

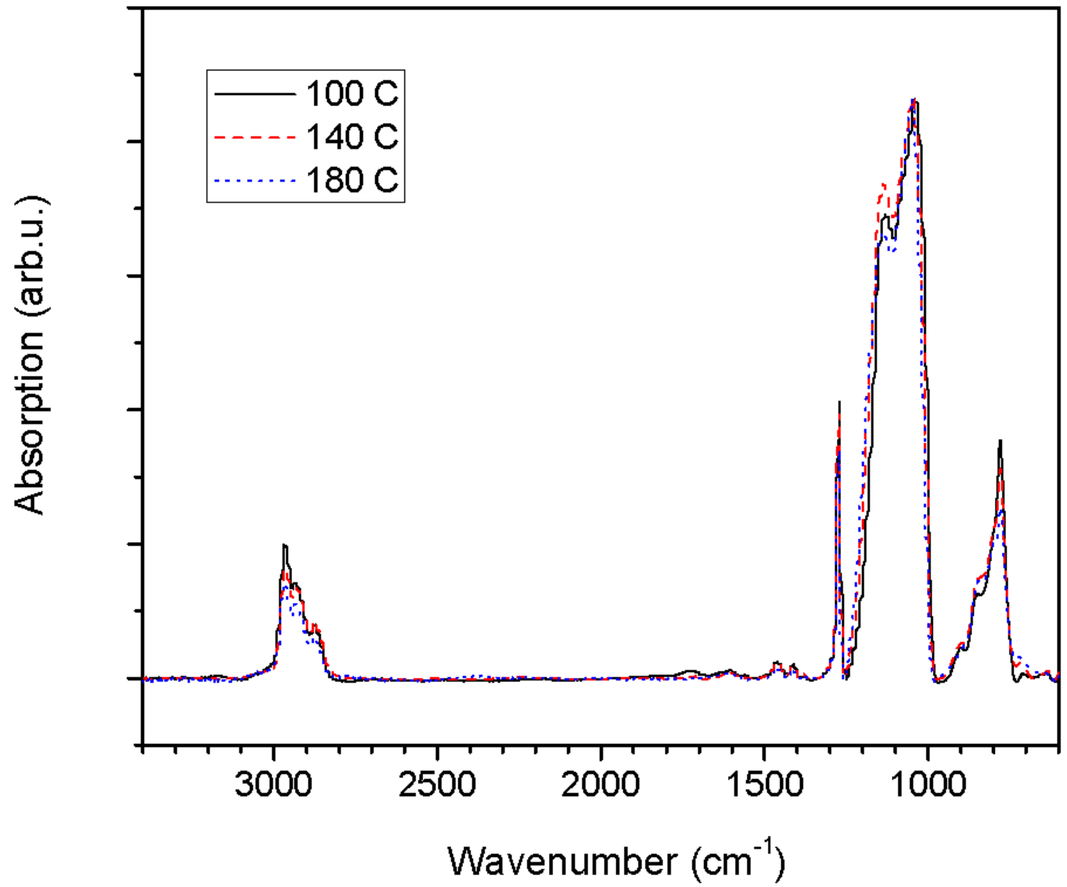
100 C
140 C
180 C
Absorption (arb.u.)
3000
2500
2000
1500
1000
Wavenumber (cm-1)

Figure 3.a

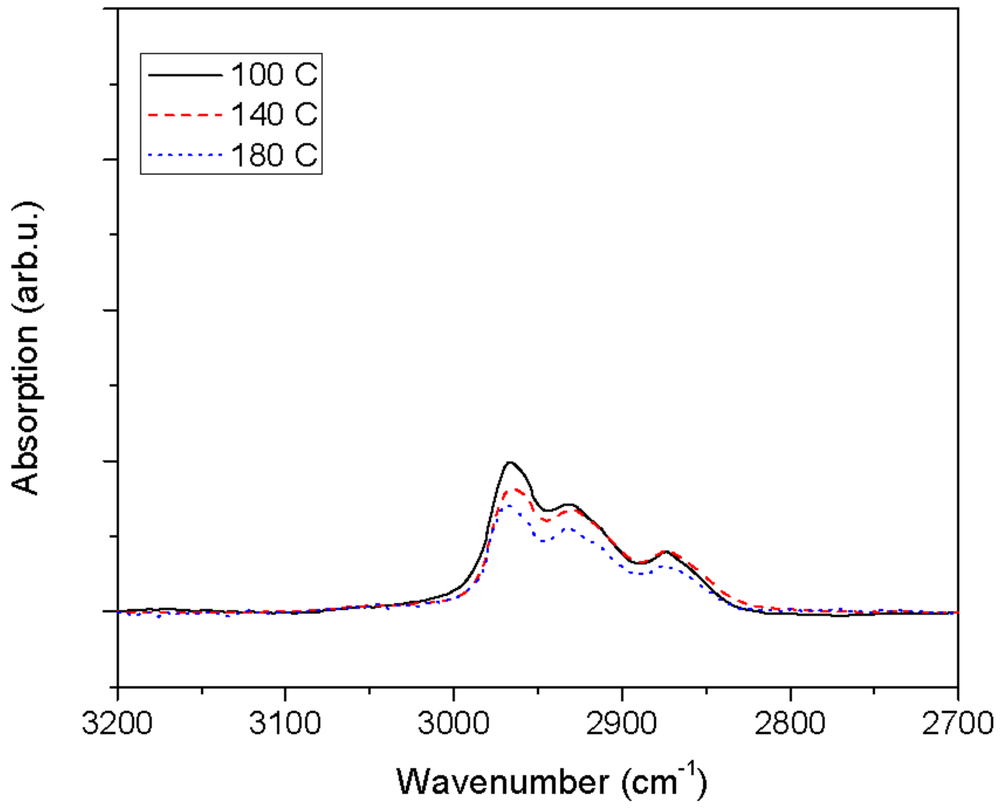
100 C
140 C
180 C
Absorption (arb.u.)
3200
3100
3000
2900
2800
2700
Wavenumber (cm-1)

Figure 3.b

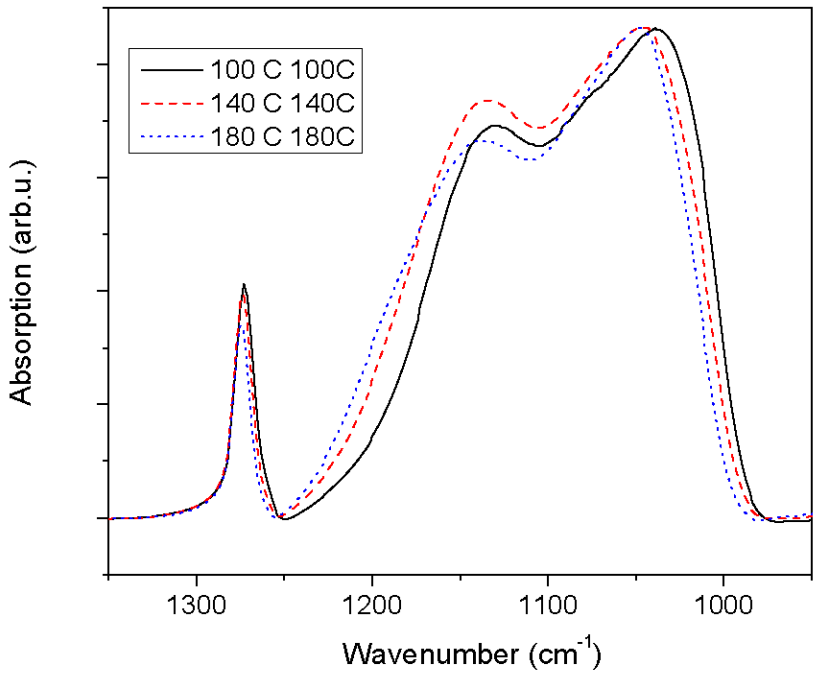
100 C 100C
140 C 140C
180 C 180C
Absorption (arb.u.)
1300
1200
1100
1000
Wavenumber (cm-1)

Figure 3.c

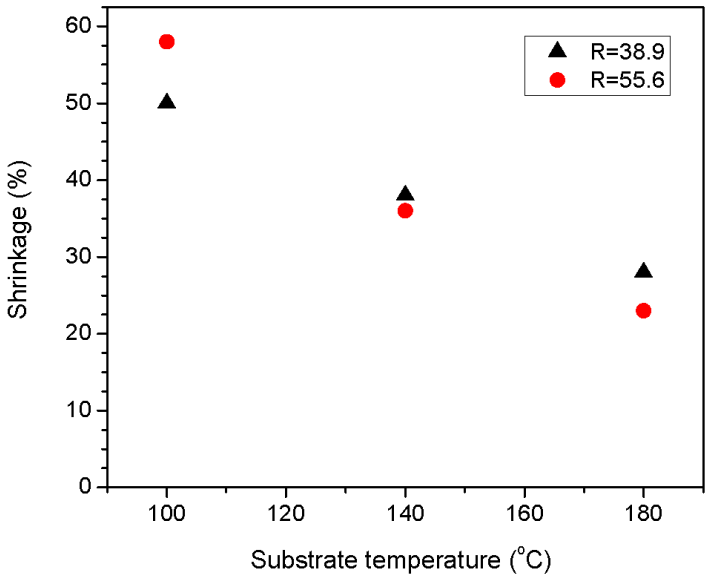
R=38.9
R=55.6
Shrinkage (%)
Substrate temperature (°C)
0
10
20
30
40
50
60
100
120
140
160
180

Figure 4

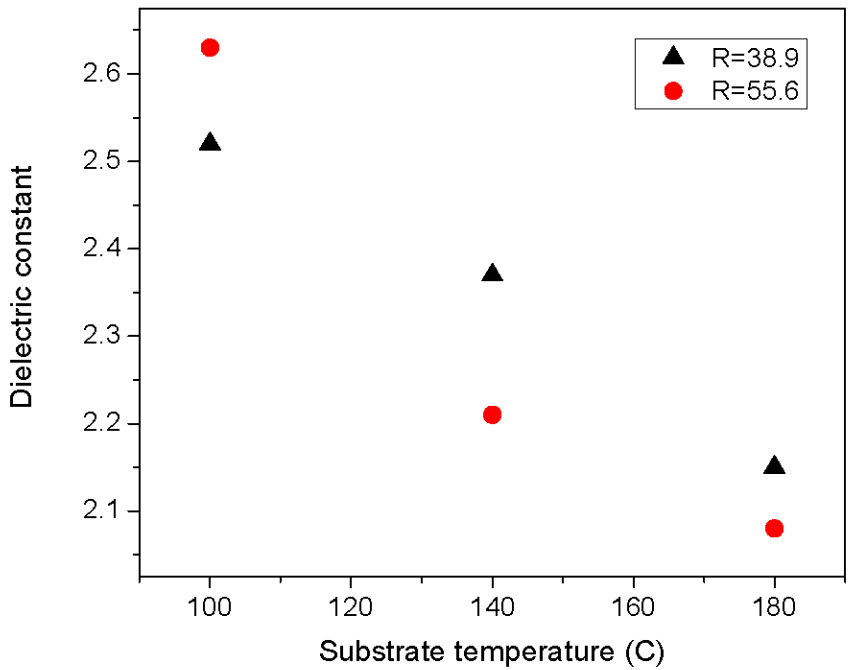
R=38.9
R=55.6
Dielectric constant
2.6
2.5
2.4
2.3
2.2
2.1
100
120
140
160
180
Substrate temperature (C)

Figure 5

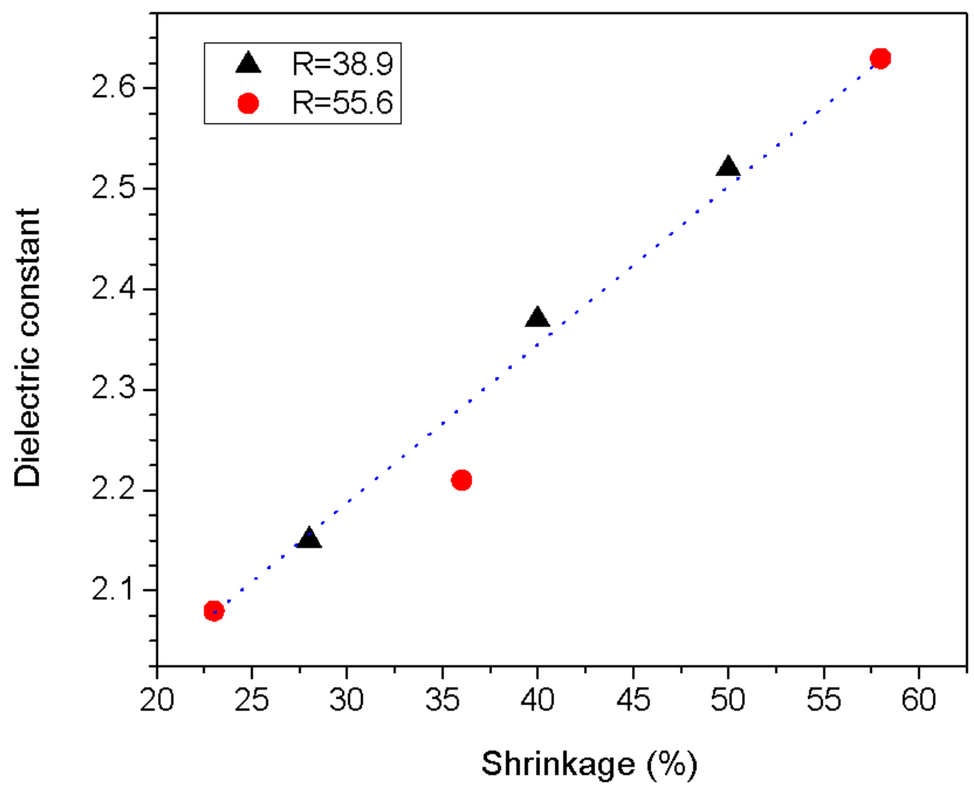
R=38.9
R=55.6
Dielectric constant
2.1
2.2
2.3
2.4
2.5
2.6
20
25
30
35
40
45
50
55
60
Shrinkage (%)

Figure 6

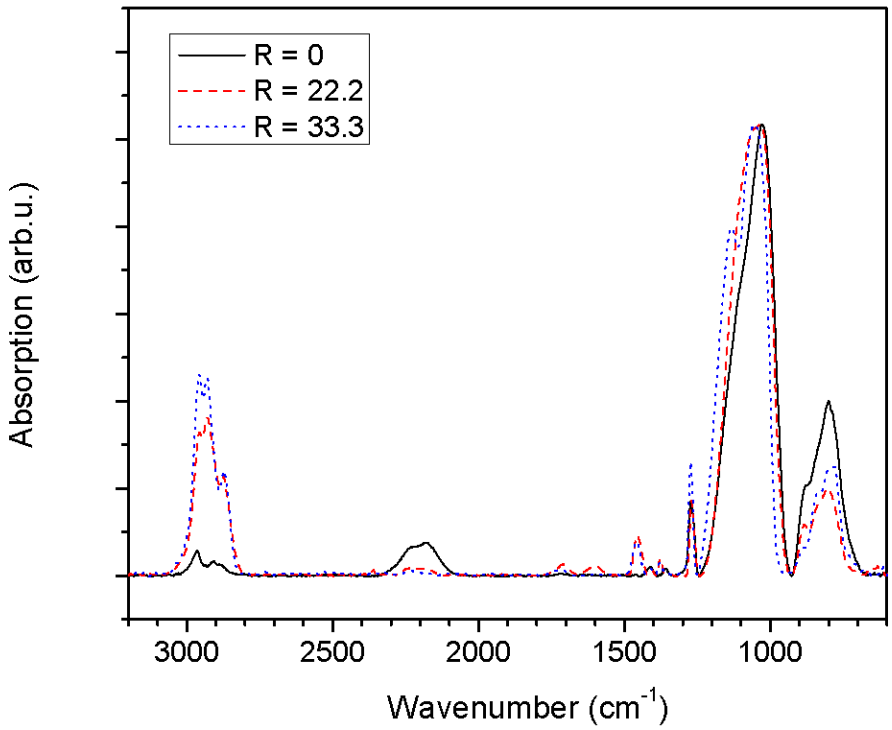
R = 0
R = 22.2
R = 33.3
Absorption (arb.u.)
3000
2500
2000
1500
1000
Wavenumber (cm-1)

Figure 7.a

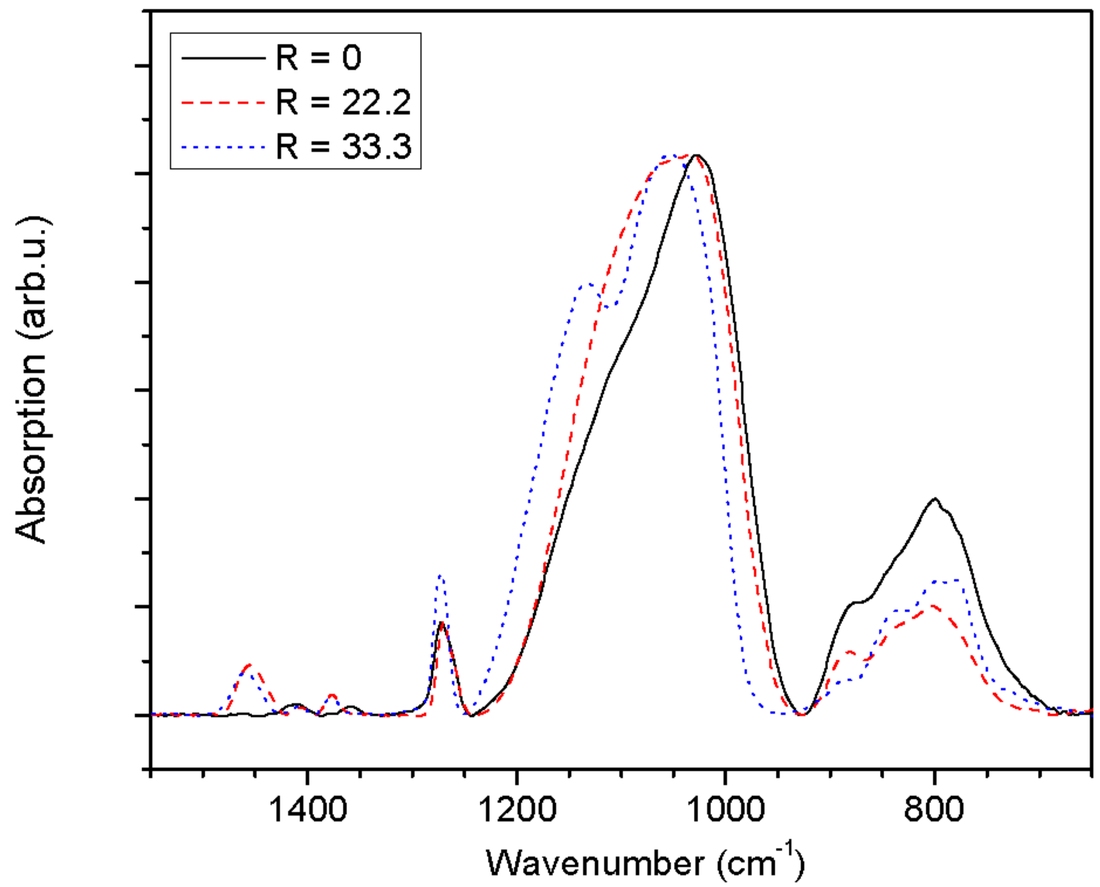
R = 0
R = 22.2
R = 33.3
Absorption (arb.u.)
1400
1200
1000
800
Wavenumber (cm-1)

Figure 7.b

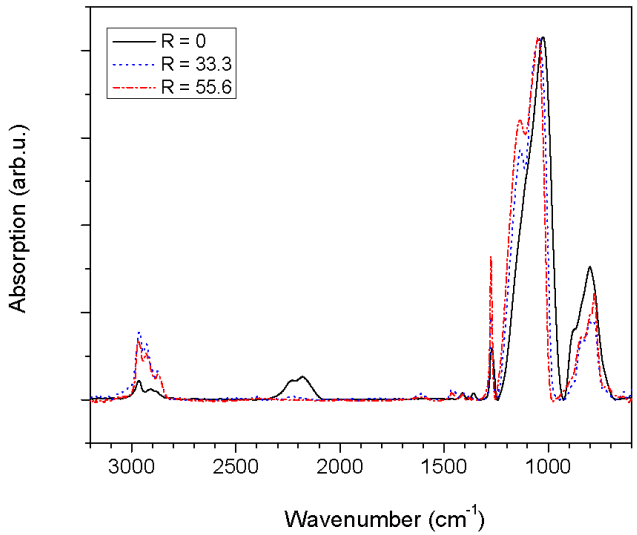
R = 0
R = 33.3
R = 55.6
Absorption (arb.u.)
3000
2500
2000
1500
1000
Wavenumber (cm-1)

Figure 8.a

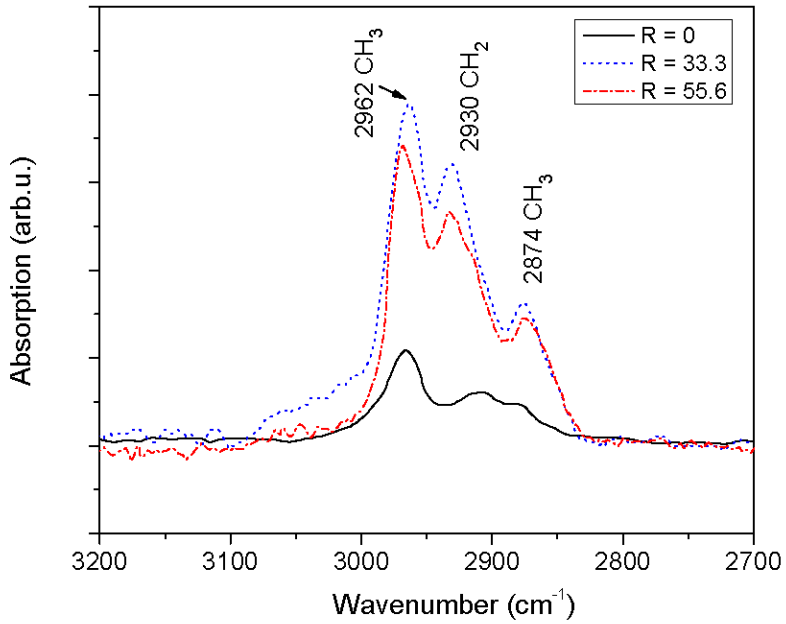
R = 0
R = 33.3
R = 55.6
2962 CH3
2930 CH2
2874 CH3
Absorption (arb.u.)
3200
3100
3000
2900
2800
2700
Wavenumber (cm-1)

Figure 8.b

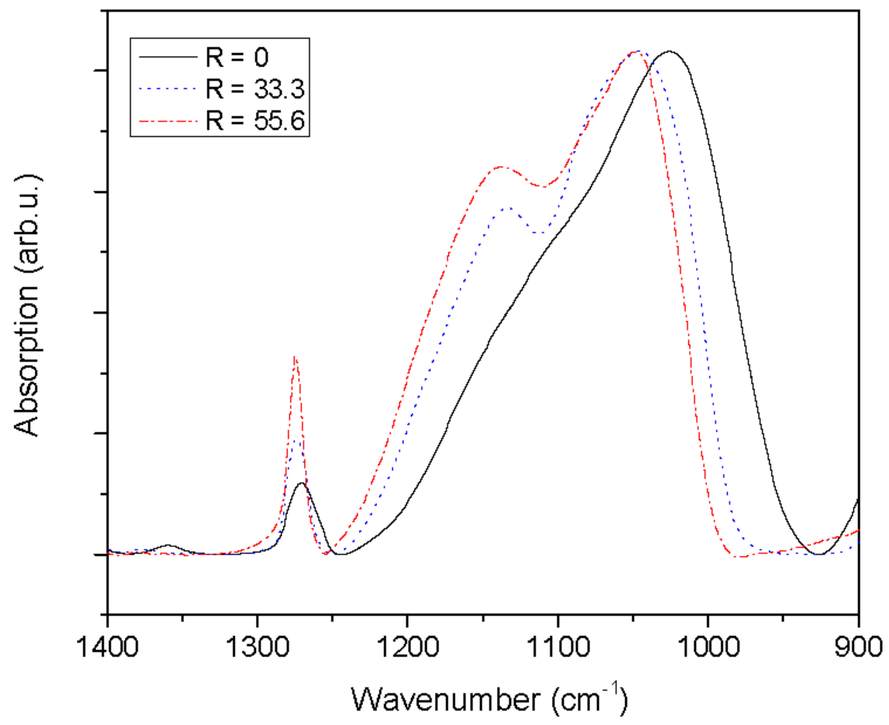
R = 0
R = 33.3
R = 55.6
Absorption (arb.u.)
1400
1300
1200
1100
1000
900
Wavenumber (cm-1)

Figure 8.c

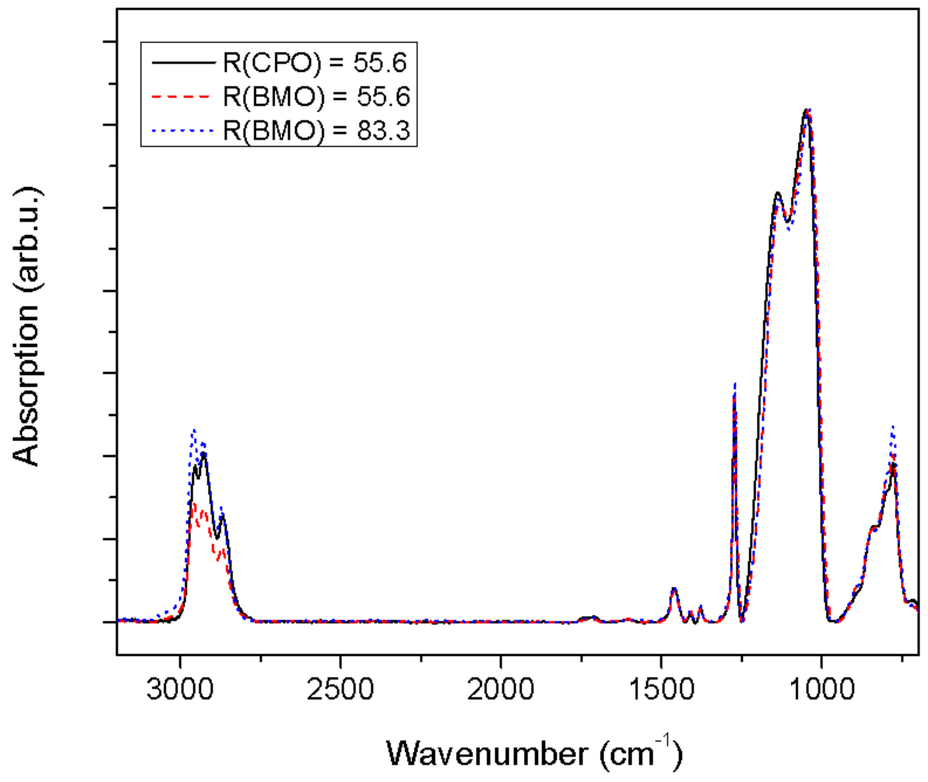
R(CPO) = 55.6
R(BMO) = 55.6
R(BMO) = 83.3
Absorption (arb.u.)
3000
2500
2000
1500
1000
Wavenumber (cm-1)

Figure 9.a

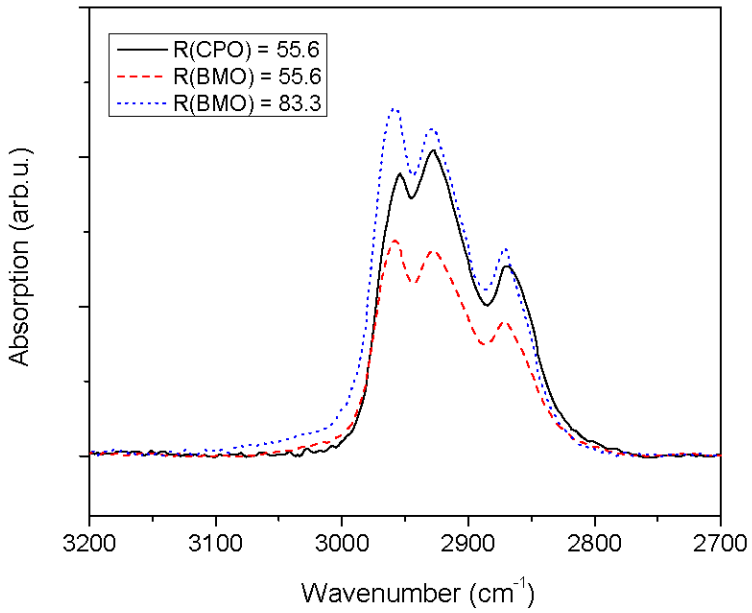
R(CPO) = 55.6
R(BMO) = 55.6
R(BMO) = 83.3
Absorption (arb.u.)
3200
3100
3000
2900
2800
2700
Wavenumber (cm-1)

Figure 9.b

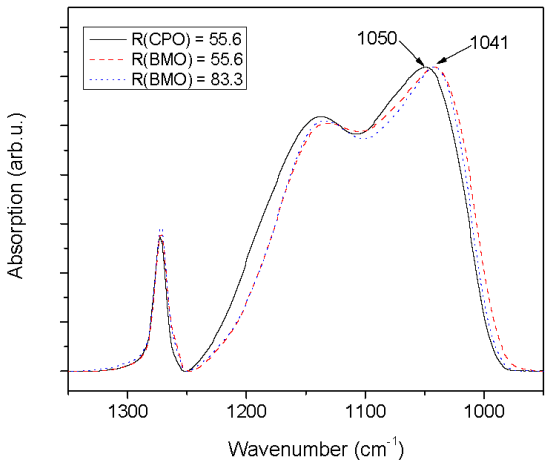
R(CPO) = 55.6
R(BMO) = 55.6
R(BMO) = 83.3
1050
1041
Absorption (arb.u.)
1300
1200
1100
1000
Wavenumber (cm-1)

Figure 9.c

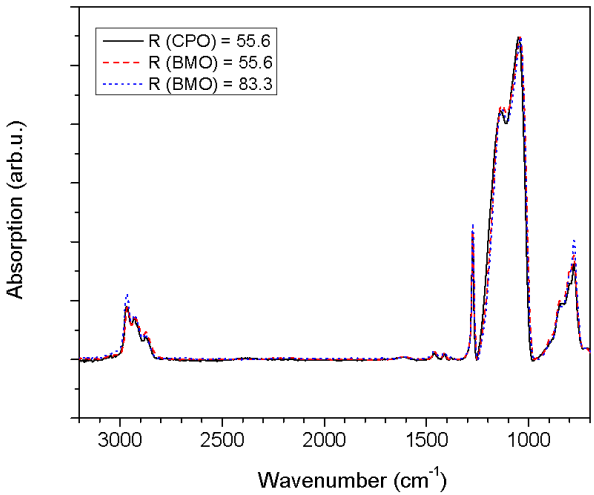
R (CPO) = 55.6
R (BMO) = 55.6
R (BMO) = 83.3
Absorption (arb.u.)
3000
2500
2000
1500
1000
Wavenumber (cm-1)

Figure 10.a

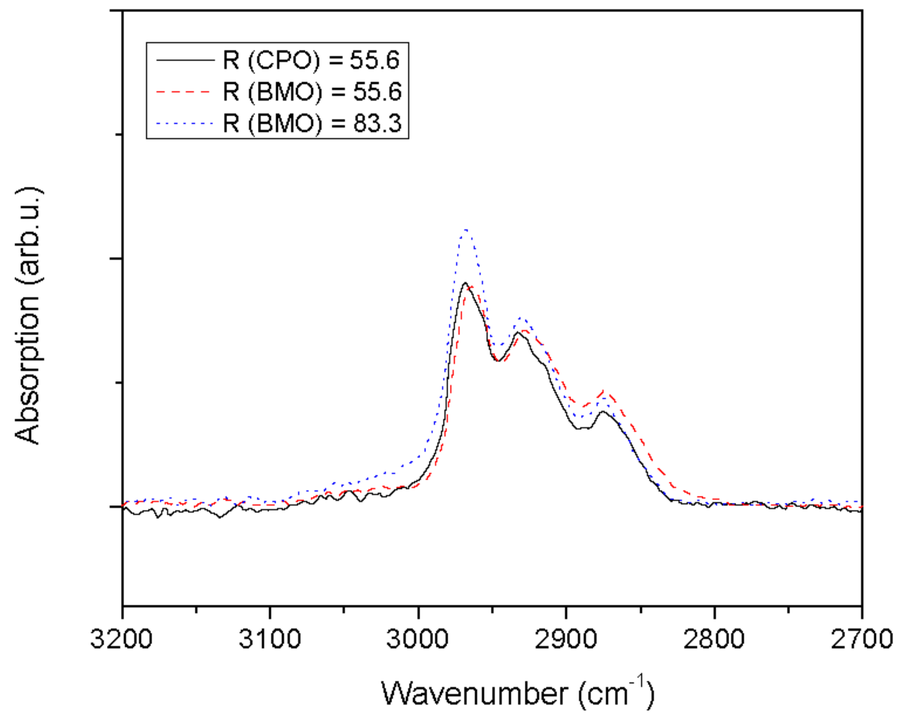
R (CPO) = 55.6
R (BMO) = 55.6
R (BMO) = 83.3
Absorption (arb.u.)
3200
3100
3000
2900
2800
2700
Wavenumber (cm-1)

Figure 10.b

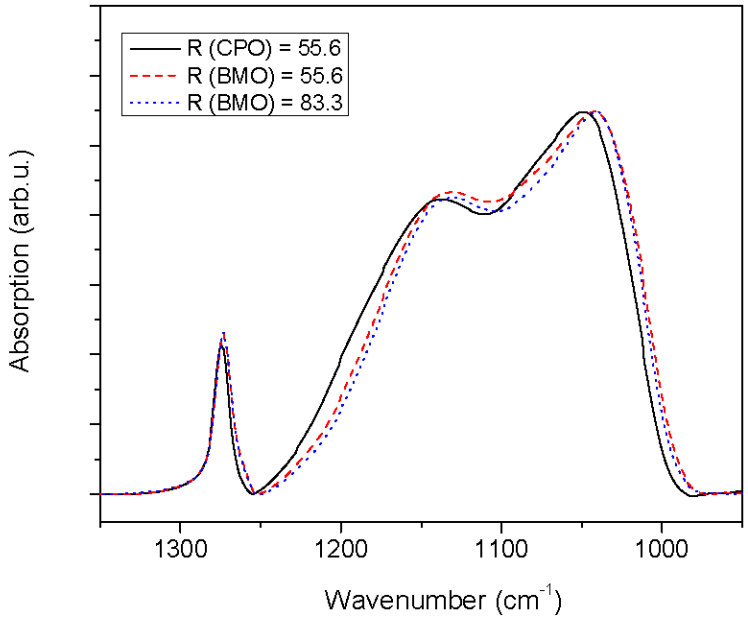
R (CPO) = 55.6
R (BMO) = 55.6
R (BMO) = 83.3
Absorption (arb.u.)
1300
1200
1100
1000
Wavenumber (cm-1)

Figure 10.c

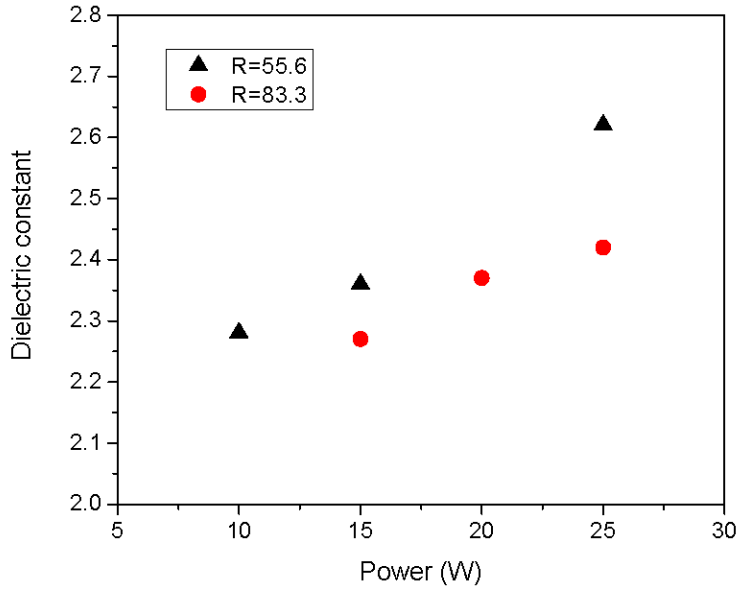
R=55.6
R=83.3
Dielectric constant
Power (W)
2.8
2.7
2.6
2.5
2.4
2.3
2.2
2.1
2.0
5
10
15
20
25
30

Figure 11

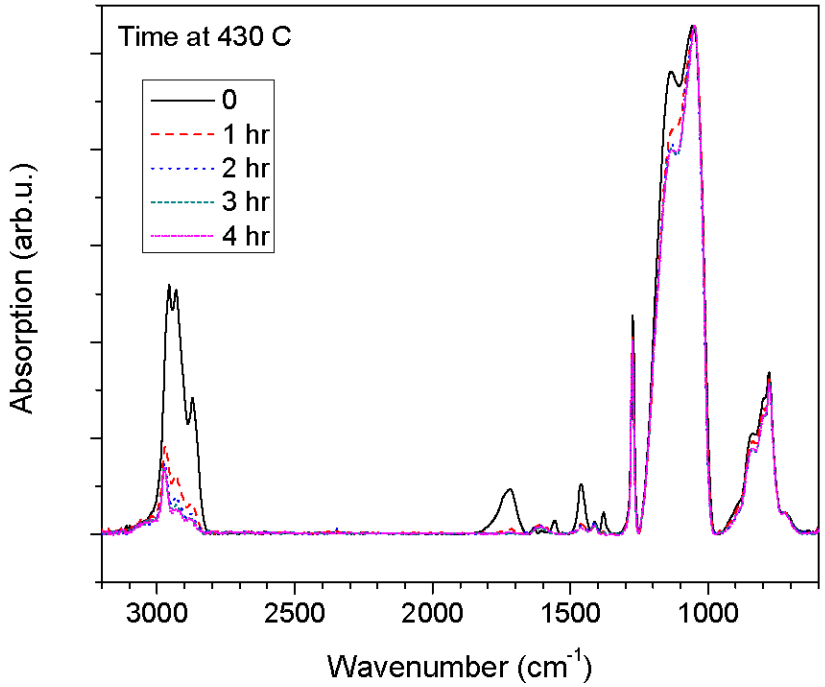
Time at 430 C
0
1 hr
2 hr
3 hr
4 hr
Absorption (arb.u.)
3000
2500
2000
1500
1000
Wavenumber (cm-1)

Figure 12.a

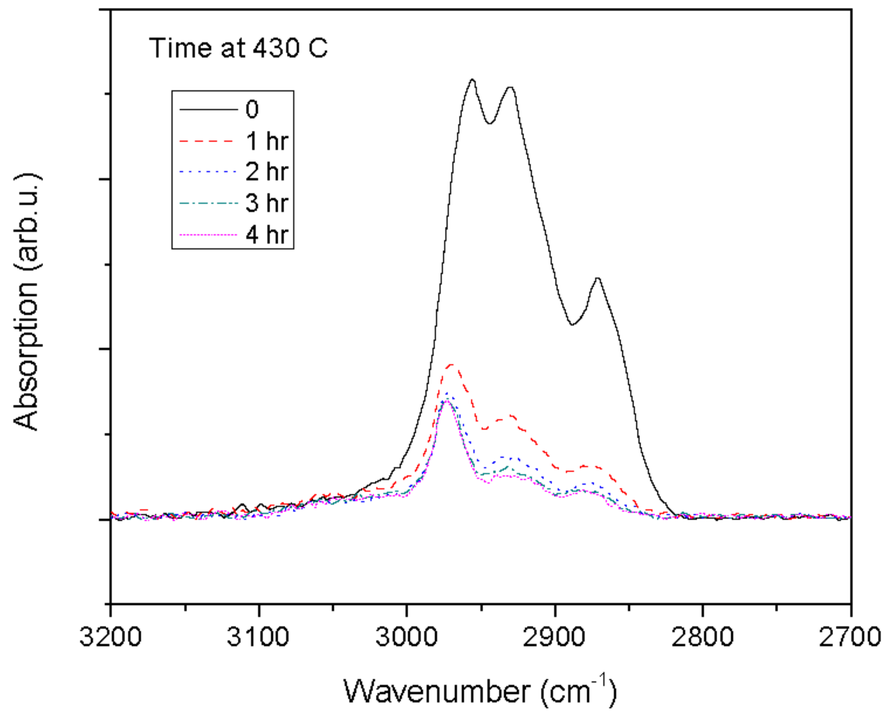
Time at 430 C
0
1 hr
2 hr
3 hr
4 hr
Absorption (arb.u.)
3200
3100
3000
2900
2800
2700
Wavenumber (cm-1)

Figure 12.b

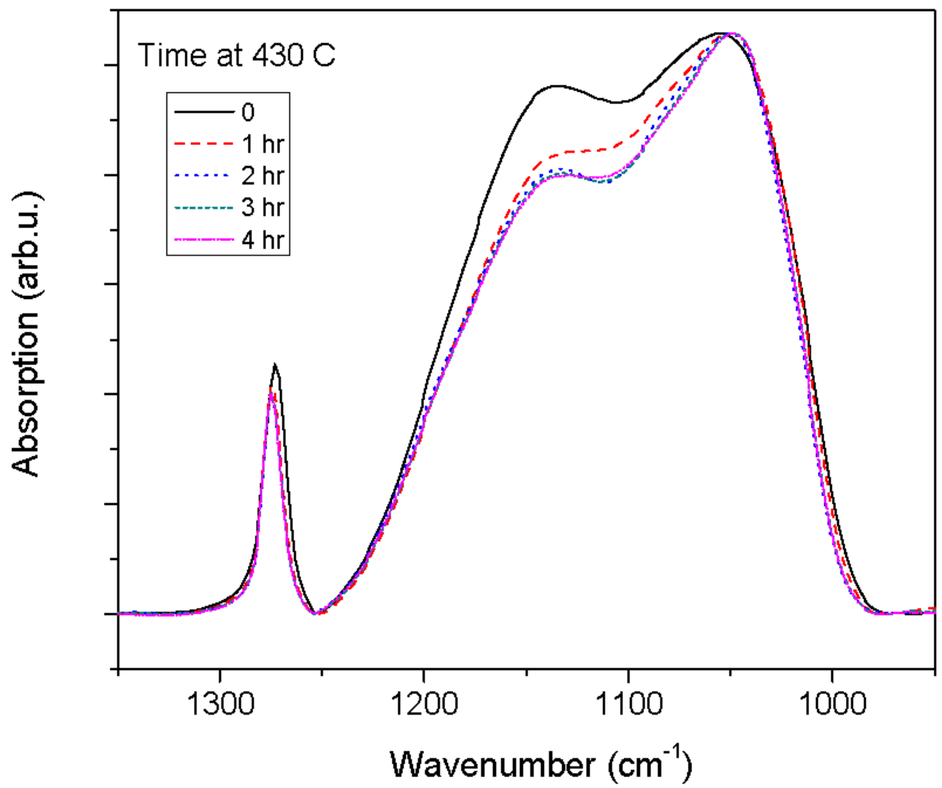
Time at 430 C
0
1 hr
2 hr
3 hr
4 hr
Absorption (arb.u.)
1300
1200
1100
1000
Wavenumber (cm-1)

Figure 12.c